Chalcogenide Letters Vol. 18, No. 11, November 2021, p. 693 - 700

Tuning visible emission of core-shell nanostructure by exchange the inner and outer layer

K. Thiruppathi[a], G. Murugadoss[b,*], M. Rajesh Kumar[c], A. Kathalingam[d,e], J. Pappannan[e], R. Jothi Ramalingam[f], Hamad Al-Lohedan[f]
[a]*Department of Physics, SRM Valliammai Engineering College, SRM Nagar Kattan Kulathur, Chennai, Tamil Nadu, India*
[b]*Centre for Nanoscience and Nanotechnology, Sathyabama Institute of Science and Technology, Chennai 600119, Tamil Nadu, India*
[c]*Institute of Natural Science and Mathematics, Ural Federal University, Yekaterinburg 620002, Russia.*
[d]*Millimeter-wave Innovation Technology Research Center, Dongguk University-Seoul, Seoul 04620, South Korea.*
[e]*Department of Genetic Engineering, School of Bioengineering, SRM Institute of Science and Engineering, SRM Nagar Kattan Kulathur, Chennai, Tamil Nadu, India.*
[f]*Department of Chemistry, College of Science, P.O. Box 2455, Kind Saud University, Riyadh 11451, Saudi Arabia*

Herein, we report that synthesis of ZnS/Bi_2S_3 and Bi_2S_3/ZnS core-shell nanostructure prepared by 'one-pot' chemical method. We have studied the effect of structural, morphological, optical and thermal properties by exchanging the inner and outer layer of core-shell nanoparticles. The samples were studied using various characterization techniques such as XRD, TEM, FTIR, UV–Vis, Photoluminescence and TG-DTA. The XRD and TEM results demonstrated that the synthesized core-shell nanoparticles were in cubic (ZnS)-orthorhombic (Bi_2S_3) mixed crystal structures with a diameter of 18.6 nm and 16.3 nm with extremely monodispersing. The obtained result provides a new and simple route for synthesis of sulfide-based core-shell nanoparticles with high crystal quality.

(Received August 8, 2021; Accepted November 5, 2021)

Keywords: Optical property, ZnS/Bi_2S_3, Core-shell, Band gap, Photoluminescence

1. Introduction

The semiconductor nanostructure materials are of great importance in several technological applications due to their electronic, photoluminescence, optical and thermal properties. In field of nanotechnology the fabrication and design of metal-oxide nanoparticles with sulphide is very great importance due to its tuneable properties for advanced applications and quantum size and surface effects [1-2]. The semiconductor-based nanoparticles such as ZnS, Bi_2S_3 CdS, CdS/Bi_2S_3, CdSe, CdSe/Bi_2S_3 CdS/Fe_3O_4, CdS/TiO_2, ZnO/CdS, ZnO/ZnS, $CdIn_2S_4$, Ag_2S, Ag_2S/SiO_2, Ag_2S/TiO_2, Bi_2S_3, NiS, CoS, CuS, HgS and PbS have been extensively studied involved in electronics, LED, luminescence, electroluminescence, flat panel displays, infrared windows, sensors, biosensors, lasers, bio-devices and catalytic applications [3–15]. Among the metal sulfieds, the ZnS and Bi_2S_3 is considered an important material, because of its structural stability, tunable band gap resulting to diverse applications [16–19]. It is well known that the bulk ZnS is an important and favourable direct semiconductor with wide band gap (~3.64 eV), high refraction index (~1.65), and high visible light transmittance [20]. The metal sulphide composite materials have tremendous luminescence property with wide band gaps have been investigated for a long time [21], because, this investigation provides exact information about the electronic positions of the energy states in the band [22]. Luminescence properties of the semiconductor

* Corresponding author: murugadoss_g@yahoo.com
https://doi.org/10.15251/CL.2021.1811.693

compound that ZnS and Bi_2S_3 were explores like thermo-luminescence, photoluminescence, optical absorption, electro-luminescence [23-25], and so on. But, not studied optical behaviours with combination of the compounds like ZnS-Bi_2S_3 composite or in a core-shell structure. Several methods have been developed to prepare semiconductor nanoparticles using physical and chemical methods, such as liquid microwave irradiation, reverse micelles, chemical vapour deposition, solid-liquid chemical reactions under co-precipitation, solvothermal and hydrothermal techniques [26-30] to synthesize of metal sulfide nanoparticles. Among the methods, 'one-pot' chemical synthesis is a facile and adoptable for synthesise in large-scale.

In recent years, increasing attention on synthesis of quantum dots (QDs) or core-shell nanoparticles for the development of luminescent probes for sensing applications [31, 32]. From the reported techniques, fluorescent sensors present many appealing advantages over the other techniques, including high sensitivity, low cost, easy detection, and remote control [33–39]. So far, however, the studies on the synthesis of nanosized structures with metal complexes as precursors have been less reported [40, 41]. The way using precursors may be helpful to manipulate the structure, purity, morphology, optical and luminescent properties of nanomaterials. In this paper, ZnS/Bi_2S_3 and Bi_2S_3/ZnS were synthesized using a simple 'one-pot' chemical synthesis. The prepared ZnS/Bi_2S_3 and Bi_2S_3/ZnS core-shell nanoparticles were characterized by several physicochemical techniques such as XRD, TEM, FTIR, UV-visible, PL and TG-DTA. The optical properties of ZnS/Bi_2S_3 and Bi_2S_3/ZnS core-shell nanoparticles were tuned by modifying the compound position.

2. Experimental details

In a typical synthesis of ZnS/Bi_2S_3 core-shell nanoparticles, 0.2M of Zn $(CH_3COO)_2.2H_2O$, in 100 mL of deionized water and an equal molar amount of sodium sulfide solution in 50 ml was added drop by drop into the above solution. Before that, 1g of PVP was used as surfactant to control the particles size. The mixture was stirred magnetically at 80 °C until a homogeneous yellow solution was obtained. Then, 0.2M of 50mL of Bismuth (III) nitrate (Bi $(NO_3)_3$) solution was added dropped into the above solution. After 5 min, the same molar concentration of 50 mL of sodium sulfide solution was added drop by drop into the above colloidal solution with continuous stirring. After 1h string of the above mixed solution, the resultant precipitate was collected and purified by washing deionized water, acetone and ethanol to remove impurities. Then, the final product was dried in a hot air oven at 160° for 2h. To synthesis of Bi_2S_3/ZnS core-shell nanoparticles, the above experimental procedure was used in reversely.

2.1. Characterization

X-ray diffraction (XRD) patterns of the powdered samples were recorded using Rigaku miniFlex IIC diffractometer with Cu Ka radiation (Kα = 1.54060 A°). The morphology and size of the nanoparticles were studied using TEM (Technai 20G2, FEI) microscopy. The functional groups of samples were identified by FT-IR using an AVATOR 360 spectrometer. UV-Vis absorption spectra of the samples were recorded using SHIMADZU UV-3101PC UV–Visible spectrophotometer. Fluorescence measurements were taken using a spectrophotometer (RF-5301PC). Thermogravimetric and differential thermal analyses (TG–DTA) were performed in air at a heating rate of 10° C/min using a SDT Q600 20 thermometer.

3. Results and discussion

3.1. X-ray diffraction

The XRD patterns of ZnS/Bi_2S_3 and Bi_2S_3/ZnS core-shell nanoparticles are showed in the Fig. 1. The crystalline nature of the prepared core-shell nanoparticles clearly seen in the XRD pattern. The ZnS has two structural components, one is cubic Zinc Blend (ZB) and other one is hexagonal [42]. The characteristic peaks for ZnS confirmed as cubic structure ((JSPDS card no.77-2100). The strong diffraction peak position of the ZnS were found at 29.34°, 26.82° and 58.92°

corresponds to (1 1 1), (2 2 0) and (3 1 1) planes. The crystal structure of Bi_2S_3 was confirmed through the JCPDS (17-0320) data. The diffraction peaks for Bi_2S_3 observed at 22.38°, 23.112°, 25.83°, 26.05°, 29.75°, 33.04°,34.02°, 35.21°, 38.24°, 43.82°, 48.72°, 54.21 and 67.62° with corresponds to (1 1 0), (0 0 2), (2 1 0), (2 2 0), (2 0 0), (1 3 2), (3 1 2), (1 1 2), (0 1 2), (0 3 4), (1 2 3), (0 3 2) and (1 7 2) planes, respectively. The all the strong diffraction peaks are confirmed that orthorhombic crystal structure of Bi_2S_3 [43]. No impurity peaks were detected for both samples indicating that core-shell nanoparticles are only composed of ZnS and Bi_2S_3 phases. The observed mixed planes of the both samples are clearly demonstrated that formation of the mixed crystal structure (Cubic-Orthorhombic). The crystallite size of the ZnS calculated using Debye-Scherrer's equation:

$$D = (K\lambda) / (\beta \cos\theta)$$

where, D is the particle size, K = 0.95 (constant), β is full width half maxima (FWHM). The calculated size of ZnS/Bi_2S_3 and Bi_2S_3/ZnS core-shell nanoparticles is 18.6 nm and 16.3 nm, respectively.

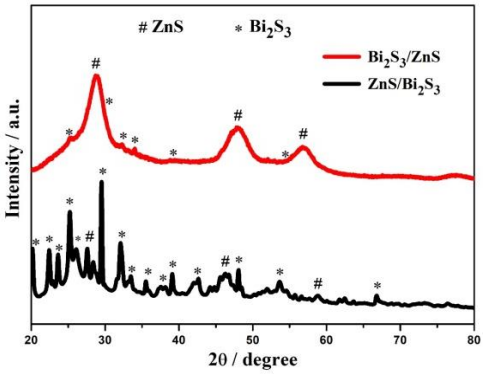

Fig. 1 X-ray diffraction spectra of zinc sulfide-bismuth sulfide (ZnS/Bi_2S_3) and bismuth sulfide-zinc sulfide (Bi_2S_3/ZnS) core shell nanoparticles. The asterisks (*) represents orthorhombic crystal structure of the Bi_2S_3 and asterisks (#) represents cubic structure of the ZnS.

The diffraction planes of ZnS/Bi_2S_3 core-shell nanoparticle exhibits more sharp peaks than the Bi_2S_3/ZnS core-shell nanoparticle. The reason behind the peaks of Bi_2S_3 nanoparticle completely covers by the ZnS particle, so the diffraction takes place over the Bi_2S_3 compound, as a result, more numbers of peaks obtained related to the Bi_2S_3. On the other hand, limited diffraction peaks found for Bi_2S_3/ZnS, the most prominent peaks appeared only related to the cubic structure of ZnS because the ZnS was exist in front layer of Bi_2S_3/ZnS core-shell nanoparticles. The broad diffraction peaks of ZnS revealed that smaller particle size.

3.2. Microstructural analysis

The TEM images of ZnS/Bi_2S_3 and Bi_2S_3/ZnS core-shell nanoparticles are shown in the Fig. 2(a-b). As displayed in Fig. 2(a), the TEM image of the ZnS/Bi_2S_3 sample shows that Bi_2S_3 microspheres was forming coarse outer layer, it further confirms that the growth of small Bi_2S_3 nanoparticles on the surface of the ZnS. Similarly, the microsphere of Bi_2S_3/ZnS core-shell (Fig. 2b) structure showed that ZnS smooth layer was covered on Bi_2S_3 surface. The microscopy images are clearly showed that a formation of core-shell structure (marked by red color circle) with average size of 18 nm and 16 nm for ZnS/Bi_2S_3 and Bi_2S_3/ZnS, respectively. The magnified microscopy images are undoubtedly showed uniformed size of particles with homogeneous distribution. The monodispersing of the core-shell nanoparticles is clearly demonstrated that the introduced 'one-pot' chemical method is more adoptable for preparation of metal sulfide based core-shell nanoparticles in industrial-scale with controlled size.

3.3. FTIR Analysis

The Fig. 3 shows the FTIR spectra of ZnS/Bi_2S_3 and Bi_2S_3/ZnS core-shell nanoparticle. For the ZnS/Bi_2S_3 (Fig. 3), the peaks appeared at 3445 cm^{-1}, 1645 cm^{-1}, 1402 cm^{-1} and 1116 cm^{-1} are assigned to O-H stretching in moisture absorbed by H_2O molecules, C-C stretching in aromatics, C-N stretching and C-O stretching in carboxyl groups, respectively. The peaks appear at 2955 cm^{-1}, 2334 cm^{-1} corresponds to the absorption of C=N, C=C, which proves that organic compound (PVP) was used during the preparation. The peaks appear at 815 cm^{-1} and 706 cm^{-1} attributed to the surface phonon modes of ZnS/Bi_2S_3, indicating effective coating of Bi_2S_3 on ZnS nanoparticle. This is due to coordination bond between the zinc ions, bismuth and sulphide ions. The peaks are observed for the Bi_2S_3/ZnS core-shell are slightly shifted towards lower frequency compared to the ZnS/Bi_2S_3. The slight shifting with reduced intensity of the peaks is due to the formation of ZnS nanoclusters on the Bi_2S_3, and reduced vibrations of bismuth and zinc ions.

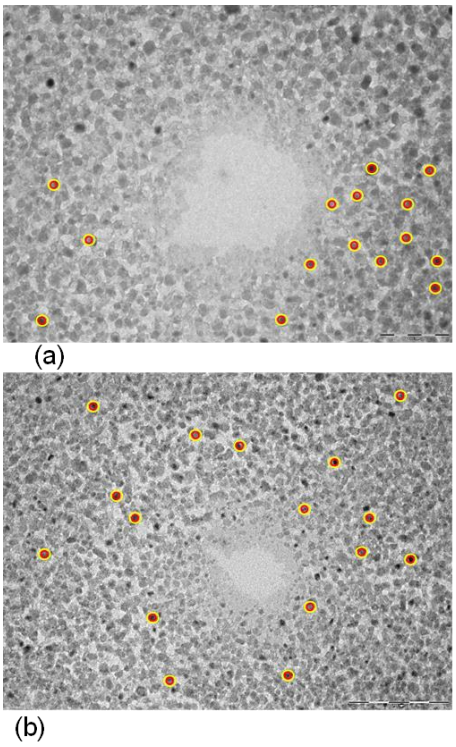

Fig. 2 (a) TEM image of the ZnS/Bi_2S_3 core shell nanoparticles, (c, d) Bi_2S_3/ZnS core shell nanoparticles. The core and shell of the nanoparticles marked by red (ZnS) and yellow (Bi_2S_3) color.

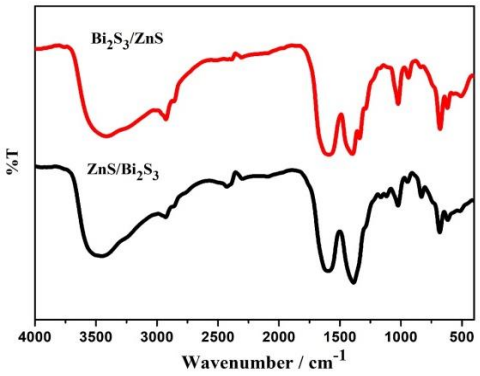

Fig. 3. FT-IR spectra of the ZnS/Bi_2S_3 and Bi_2S_3/ZnS core shell nanoparticles using KBr pellet technique.

3.4. UV-Visible absorption

The advantages of optical studies are observing the required characteristics of nanoparticles without changing significantly its nature either by non-content or non-invasive. The ultra-sensitive nature of the nanoparticles is ideal like optical sensing, optoelectronic devices to understand the semiconductor nanocrystal performance the optical absorption study is very important. Therefore, the as prepared ZnS/Bi_2S_3 and Bi_2S_3/ZnS core-shell nanoparticle was subjected to UV-visible study. The Fig. 4a shows absorption spectra obtained at room temperature in the wavelength range of 200 nm – 800 nm. The UV-visible absorption peaks those attributed to photo-induced electrons-holes separations in the core-shell nanoparticles and rapid capture of those electrons by the defects on the surface of the core-shell structure. A maximum absorption peak appeared in the spectral range of 300 nm to 500 nm. When comparing to the Bi_2S_3/ZnS, the absorption of ZnS/Bi_2S_3 shifted towards longer wavelength region. These results are clearly demonstrated that two samples have suitable band gaps, which are able to be activated by visible-light for the photocatalytic decomposition of organic dyes and optoelectronic applications. So that the nature and optical band gap values can be calculated from the fundamental absorption values, which is really means to that the electronic excitation from valence band to the conduction band. The band gap of the core-shell nanoparticle was calculated from a Tauc plot: that is a plot of $(\alpha h\upsilon)^{1/2}$ vs Band gap (E_g) [44, 45]. It is clearly seen that the band gap of ZnS/Bi_2S_3 is 2.65 eV and 3.40 eV for Bi_2S_3/ZnS, the plot obtained, the plot obtained by extrapolating the absorption edges.

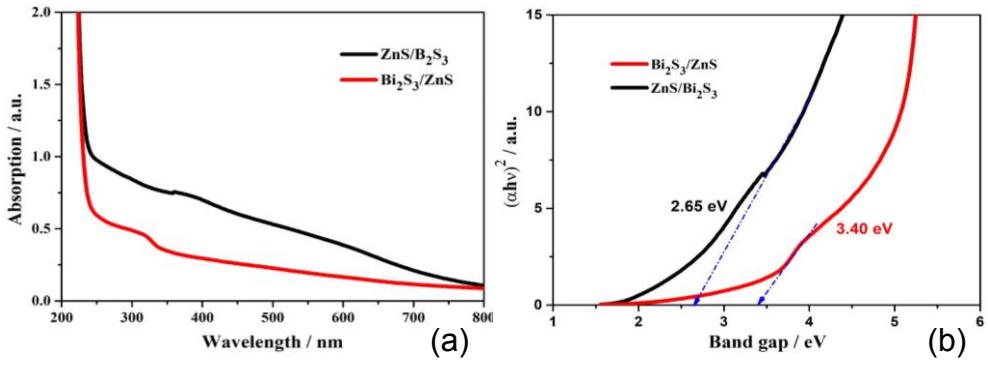

Fig. 4 (a) UV/visible absorption spectra of the ZnS/Bi_2S_3 and Bi_2S_3/ZnS core shell nanoparticles were recorded from 200 to 800 nm and (b) Tauc plot for measuring band gap of ZnS/Bi_2S_3 (3.61 eV) and Bi_2S_3/ZnS (3.75 eV) of the corresponding samples.

3.5. Photoluminescence

The important property of photoluminescence is mainly depending on the type of transition, particle size, shape, and surface energy, which influenced by surface passivation. The photoluminescence emission spectrum is a best tool, to evaluate the defects on particle surface and optical property of core-shell nanoparticles. Peak broadening in the PL emission is due to both size, particle distribution in the composition and increase in the surface energy states occurring to the increase in surface to volume ratio in the prepared core-shell nanoparticle. It can be seen that pure ZnS/Bi_2S_3 shows (Fig.5) a week broad emission band ranging from 350 to 550 nm, four primary emissions cantered at 365, 376, 425 and 475 nm. The emission at 365 nm was attributed to the typical excitonic band-to-band radiative emission of ZnS due to its location near the absorption edge. The other three peaks (Fig.5) were assigned to the trap-state emissions, presumably coming from the various point defects present in ZnS. More importantly, a significant strong PL emission (350-550 nm) was observed for the Bi_2S_3/ZnS sample as compared to ZnS/Bi_2S_3 due to more recombination of electron-hole in the surface layer. Moreover, the broad emission is due to the surface irregularity of the nanoparticles, which contains sulphur vacancies in the lattice structure [46]. Besides the emission is incurred to the electron or holes vacancies traps

in the recombination centres for photo generated charge carriers. The main advantage of these phenomena is that, the photo oxidation process which can happen on the surface of the nanoparticles. This is good advantage for fabrication of optoelectronic devices.

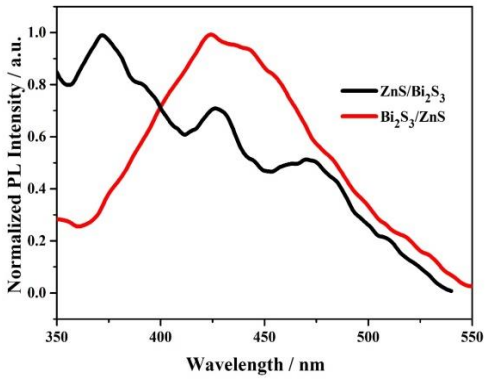

Fig. 5 shows Photoluminescence spectra of the ZnS/Bi_2S_3 and Bi_2S_3/ZnS core shell nanoparticles excited with 346 nm and 331 nm, respectively.

3.6. Thermal analysis

The thermal stability was investigated for ZnS/Bi_2S_3 core-shell nanoparticles. The sample was calcinated from room temperature to 1000 °C in a nitrogen atmosphere, with an increment of 5°C/min, as shown in the Fig. 6. The result is clearly showed few distinct weight losses in the sample due desorption of water molecule below 200 °C. In the region from 200 °C to 440 °C, drastic change in the TG curve shows which indicates the decomposition of some organic species which present on the surface of the core-shell nanoparticle. The phase transformation takes place in the region 450 °C to 700 °C (plateau region), next in the temperature range of 700 °C - 850 °C, a significant weight loss shows due to release of residual sulphur ion from the core-shell nanoparticle. A corresponding change (a hump) displayed in the DTA curve at the high temperature region. Above 850 °C, there is no change observed which indicates, there is no any residual phase loss in that region. The final percentage of weight loss of the core-shell nanoparticle is around 56% up to 850 °C. In DTA curve result, it clearly shows both endothermic as well as exothermic peaks which indicates, the occurrence of thermal decomposition and oxidative decomposition at different temperature range.

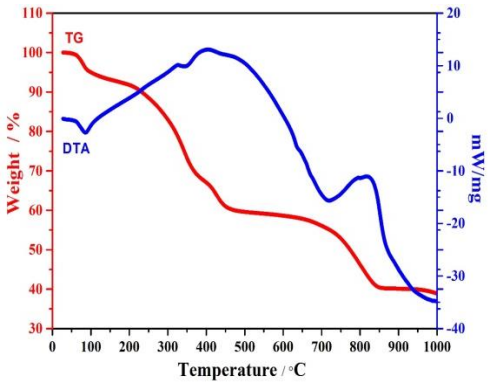

Fig. 6 TG-DTA analysis of the Bi_2S_3/ZnS core shell nanoparticles from RT to 1000˚C in nitrogen atmosphere.

4. Conclusions

Herein, well crystalline ZnS/Bi_2S_3 and Bi_2S_3/ZnS core-shell nanoparticles were successfully prepared via 'one-pot' synthesis method. The formation of the core-shell structure was confirmed by mixed crystal structure present in the XRD pattern and distinguishes formation of the outer and inner layer of the ZnS and Bi_2S_3 in the TEM microscopy images. These core-shell nanostructures show highly efficient visible-light-driven photoluminescence. The enhanced PL emission of ZnS/Bi_2S_3 core-shell nanostructures may be attributed to the effective separation of photo induced electron-hole pair carriers in the ZnS/Bi_2S_3 and which leads to the rapid capture of those electrons by the core-shell structure. This result provides very helpful insight in the design and synthesis of sulfide based highly efficient photoluminescence activity and visible-light-driven photocatalysts in future.

Acknowledgment

The authors acknowledge the Researchers Supporting Project Number (RSP-2021/354) King Saud University, for financial supports, Riyadh, Saudi Arabia. The author Dr. G. Murugadoss thanks the Chancellor, President, and Vice Chancellor, Sathyabama Institute of Science and Technology, Chennai for the support and encouragement.

References

[1] D. Ayodhya, G. Veerabhadram, Modern Electronic Materials **4**, 151 (2018).
[2] W. Xitao, L. Rong, W. Kang, J. Mater. Chem. A **2**, 8304 (2014).
[3] K. Ramki, A. RajaPriya, P. Sakthivel, G. Murugadoss, R. Thangamuthu, M. R. Kumar, J. Mater. Sci.: Mater. in Electronics **31**, 8750 (2020).
[4] G. Murugadoss, V. Ramasamy, Spectrochimica Acta Part A: Molecular and Biomolecular Spectroscopy **93**, 290 (2012).
[5] G. Murugadoss, Particuology **10**, 722 (2012).
[6] M. R. Kumar, G. Murugadoss, J. Lumin. **146**, 325 (2014).
[7] G. Murugadoss, R. Thangamuthu, R. Jayavel, M. R. Kumar, J. Lumin. **165**, 30 (2015).
[8] G. Murugadoss, Particuology **11**, 566 (2013).
[9] R. Bhadra, V.N. Singh, B.R. Mehta, P. Datta, Chalcogenide Lett. **6**, 189 (2009).
[10] D. Ayodhya, M. Venkatesham, A.S. Kumari, G.B. Reddy, D. Ramakrishna, G. Veerabhadram, J. Fluoresce. **25**(5), 1481 (2015).
[11] M. Mousavi-Kamazani, Z. Zarghami, M. Salavati-Niasari, J. Phys. Chem. C **120**, 2096 (2016).
[12] M. Sabet, M. Salavati-Niasari, O. Amiri, Electrochimica Acta **117**, 504 (2014).
[13] H. Safardoust-Hojaghan, M. Shakouri-Arani, M. Salavati-Niasari, Transactions of Nonferrous Metals Society of China **26**, 759 (2016).
[14] D. Ayodhya, G. Veerabhadram, J. Environ. Chem. Eng. **6**, 311 (2018).
[15] R. Yi, G. Qiu, X. Liu, J. Solid State Chem. **182**, 2791 (2009).
[16] E. M. Flores, C.W. Raubach, R. Gouvea, E. Longo, S. Cava, M.L. Moreira, Mater. Chem. Phys. **173**, 347 (2016).
[17] X. Yuan, X. Wu, Z. Feng, W. Jia, X. Zheng, C. Li, Catalysts **9**, 624 (2019).
[18] T. Zhang, T. Doert, M. Ruck, J. Inorg. and General Chem. **643**, 1913 (2017).
[19] B. Zeng, W. Zeng, Digest J. Nanomaterials and Biostructures **11**, 1105 (2016).
[20] J. Zhu, M. Zhou, J. Xu, X. Liao, Mater. Lett. **47**, 25 (2001).
[21] H. Sasakura, H. Kobayashi, S. Tanaka, J. Mita, T. Tanaka, H. Nakayama, J. Appl. Phys. **52**, 6901 (1981).
[22] J. Huang, Y. Yang, S. Xue, B. Yang, S. Liu, J. Shen, Appl. Phys. Lett. **70**, 2335 (1997).
[23] R. Sharma, D.P. Bisen, Luminescence **30**, 175 (2015).
[24] D. R. Frankl, Phys. Rev. **111**, 1540 (1958).

[25] W. Chen, Z. Wang, Z. Lin, L. Lin, J. Appl. Phys. **82**, 3111 (1997).
[26] P. S. Khiew, S. Radiman, N. M. Huang, S. M. Ahmed, K. Nadarajah, Mater. Lett. **59**, 989 (2005).
[27] V. G. Bessergenev, E. N. Ivanova, Y. A. Kovalevskaya, S. A. Gromilov, V. N. Kirichenko, S. M. Zemskova, I. G. Vasilieva, B. M. Ayupov, N. L. Shwarz, Mater. Res. Bull. **30**, 1393 (1995).
[28] D. Ayodhya, M. Venkatesham, A. S. Kumari, K. G. Mangatayaru, G. Veerabhadram, J. Appl. Chem. **6**, 1 (2013).
[29] J. Liu, J. Ma, Y. Liu, Z. Song, Y. Sun, J. Fang, Z. Liu, J. Alloys Compd. **486**, L40 (2009).
[30] D. Denzler, M. Olschewski, K. Sattler, J. Appl. Phys. **84**, 2841 (1998).
[31] D. Ayodhya, G. Veerabhadram, Mater. Sci. Eng. B **225**, 33 (2017).
[32] K. Rurack, U. R. Genger, Chem. Soc. Rev. **31**, 116 (2002).
[33] J. K. Huber, Analyst. **124**, 657 (1999).
[34] M. E. del Castillo Busto, M. Montes-Bayón, E. Blanco-González, J. Meija, A. Sanz-Medel, Anal. Chem. **77**, 5615 (2005).
[35] J. E. Andersen, Analyst. **130**, 385 (2005).
[36] C. M. G. van den Berg, Anal. Chem. **78**, 156 (2006).
[37] Y. Dilgin, B. Kizilkaya, B. Ertek, N. Eren, D. G. Dilgin, Talanta. **89**, 490 (2012).
[38] J. Radford-Knoery, G. A. Cutter, Anal. Chem. **65**, 976 (1993).
[39] A. Safavi, M. A. Karimi, Talanta **57**, 491 (2002).
[40] J. Ghasemi, D. M. Ebrahimi, L. Hejazi, R. Leardi, A. Niazi, J. Anal. Chem. **62**, 348 (2007).
[41] D. Ayodhya, G. Veerabhadram, J. Inorg. Organomet. Polymer Mat. **27**, 215 (2017).
[42] G. Murugadoss, R. Jayavel, R. Thangamuthu, M. R. Kumar, J. Lumin. **170**, 78 (2016).
[43] G. Murugadoss, R. Jayavel, M. Rajesh Kumar, Indian J. Phys. **90**, 173 (2016).
[44] G. Manibalan, G. Murugadoss, R. Thangamuthu, P. Ragupathy, M. R. Kumar, R. M. Kumar, R. Jayavel, Inorg. Chem. **58**, 13843 (2019).
[45] N. Kandhasamy, G. Ramalingam, G. Murugadoss, M. R. Kumar, G. Manibalan, R. JothiRamalingam, H. M. Yadav, J. Alloys Compd. **888**, 161489 (2021).
[46] G. Murugadoss, B. Rajamannan, V. Ramasamy, G. Viruthagiri, J. Ovonic Res. **5**, 107 (2009).